Catalysis Today 176 (2011) 7–13

Contents lists available at ScienceDirect

Catalysis Today

journal homepage: www.elsevier.com/locate/cattod

Supported Au catalysts for propene total oxidation: Study of support morphology and gold particle size effects

M. Ousmane[a,b], L.F. Liotta[c,*], G. Pantaleo[c], A.M. Venezia[c], G. Di Carlo[d], M. Aouine[a,b], L. Retailleau[a,b], A. Giroir-Fendler[a,b,**]

[a] Université de Lyon, Lyon, F-69003, France
[b] Université Lyon 1, Villeurbanne, F-69622, CNRS, UMR 5256, IRCELYON, 2 avenue Albert Einstein, Villeurbanne, F-69622, France
[c] Istituto per Lo Studio dei Materiali Nanostrutturati (ISMN)-CNR via Ugo La Malfa, 153, 90146 Palermo, Italy
[d] Istituto per Lo Studio dei Materiali Nanostrutturati (ISMN)-CNR, Via Salaria km 29300, 00015 Monterotondo Stazione, Roma, Italy

ARTICLE INFO

Article history:
Received 24 January 2011
Received in revised form 7 July 2011
Accepted 11 July 2011
Available online 10 August 2011

Keywords:
Au
TiO_2
ZnO
Al_2O_3
Propene oxidation
Au particle size
Metal–support interaction
Support morphology

ABSTRACT

In this work gold nanoparticles supported over three different metal oxides, TiO_2, ZnO and Al_2O_3 were characterized by BET surface area and pore size distribution, XRD, XPS and TEM techniques and their catalytic performances were evaluated in the total oxidation of propene, chosen as model VOC molecule. Attention was focused on the evaluation of the catalytic activity by performing three consecutive catalytic runs. Characterizations by XPS and TEM were carried out on the spent catalysts after propene oxidation tests.

The results were discussed in terms of relationship between morphological, structural, electronic and catalytic properties as a function of the nature of the support.

1. Introduction

Volatile organic compounds (VOCs) are an important class of air pollutants, emitted from many industrial processes and transportation activities [1]. Catalytic combustion is one of the most promising technologies for the destruction of VOCs, due to its definitive character and save of energy. Low temperature VOCs catalytic oxidation has been widely studied over nano-sized gold supported on a wide variety of metal oxides such as CeO_2, Fe_2O_3, TiO_2, ZrO_2, Al_2O_3 and Al_2O_3 doped by transition metal oxides [2–8]. When compared to the other supports, ZnO has been less used as carrier for gold catalysts [9]. Few studies have been carried out on Au/ZnO catalysts for CO oxidation [10–15] and to be used as sensor for CO and VOCs molecules [16–19]. Although, ZnO does not belong to the reducible oxides, it should be regarded as a strongly interacting support. Indeed, Au/ZnO catalysts have been demonstrated to be active in the low-temperature CO oxidation [10–15]. The occurrence of Au–ZnO interaction has been established to increase the CO oxidation activity of $Au/ZnO/SiO_2$ catalysts where gold nanoparticles nucleate on the oxygen vacancies and grain boundary defects of ZnO [15]. The effects of a strong metal–oxide interaction between Au and ZnO atomic planes have been also claimed to explain the high catalytic activity in benzene, toluene and xylene oxidation of colloidal gold supported on ZnO nanoparticles [20].

Many factors influence the catalytic activity of gold in VOC oxidation, such as Au loading and oxidation state, shape of Au particles, nature of the support (reducible and/or interacting, inert), gold/support perimeter interface [2–4,7,8,21]. Reducible oxides stabilize gold as small nanoparticles anchored at the oxygen vacancies [22,23]. Moreover, the support may influence the electronic state of gold. Au^{3+} and Au^{1+} ionic species are stabilized by reducible oxides, like titania and ceria [24,25]. On the contrary when a non-reducible and inert oxide, like silica or alumina, is used gold interacts weakly with the support, its use resulting in gold agglomeration and low catalytic activity [26,27].

The use of a mesoporous oxide with a well defined pore size seems to be an ideal candidate in order to obtain a strong confinement of metal nanoparticles.

* Corresponding author at: ISMN-CNR, Palermo, Italy. Tel.: +39 091 6809371.
** Corresponding author at: Université Lyon 1, Villeurbanne, F-69622, CNRS, UMR 5256, IRCELYON, 2 avenue Albert Einstein, Villeurbanne, F-69622, France. Tel.: +33 472 431586.
E-mail addresses: liotta@pa.ismn.cnr.it (L.F. Liotta), anne.giroir-fendler@univ-lyon1.fr (A. Giroir-Fendler).

0920-5861/$ – see front matter © 2011 Elsevier B.V. All rights reserved.
doi:10.1016/j.cattod.2011.07.009

Accordingly, in the last few years, the use of ordered mesoporous silica, like MCM-41, MCM-48, SBA-15 and wormhole HMS oxide, has been widely addressed as carriers for gold deposition. The porous structure, in terms of pore diameter (ranging between 2 and 8 nm) and wall thickness, strongly influenced the CO oxidation activity and stability of gold nanoparticles [28,29]. Functionalization of the silica support by organo-silanes [28,30,31] or by TiO_2, CeO_2 oxides [29,32,33] displayed a better confinement of gold nanoparticles inside the porous structure and increased their catalytic performances.

However, depending on the support morphology, contradictory results have been reported on the activity of supported nanoparticles and accessibility of reactants. The support porosity has been evoked to explain the decreased activity of small sized gold nanoparticles over ceria, embedded within the porous structure of the matrix [34].

The purpose of the present work was to investigate the morphological, structural, electronic, and catalytic properties in propene oxidation of industrial Au catalysts (supplied by Mintek) deposited over three different types of supports, TiO_2, ZnO and Al_2O_3 characterized by surface area of ~50 m^2/g for titania and zinc oxide, 253 m^2/g for alumina and pore diameter ranging between 10 and 30 nm. The catalysts were characterized by specific surface area measurements (BET method) and pore size distribution, X-ray diffraction (XRD), transmission electron microscopy (TEM) and X-ray photoelectron spectroscopy (XPS) techniques. The maintenance of the catalytic activity by performing three consecutive runs in propene oxidation was evaluated. To evaluate the catalysts modification upon reaction, analyses by XPS and TEM techniques were performed on the spent samples.

2. Experimental

2.1. Catalysts preparation

Three different Au(1 wt%) catalysts (AURO*lite*™) supported over TiO_2, ZnO and Al_2O_3 were supplied by Mintek Corporation [35]. Gold was introduced by deposition–precipitation (DP) method starting from aqueous solution of $HAuCl_4$ at pH of 7. The dispersion was aged at 70 °C for 1 h and was washed with distilled water several times. The catalysts were dried in air at 120 °C for 5 h, then reduced in 5%H_2/N_2 at 120 °C for 1 h (fresh catalysts). Hydrogen treatment at 120 °C is known to reduce gold in small nanoparticles stabilizing them against sintering in oxidative treatment at higher temperature [36,37].

2.2. Catalysts characterization

The specific surface areas of the catalysts were determined by the BET equation from nitrogen adsorption isotherms at −196 °C using Sorptomatic 1900 (Carlo Erba) instrument. The mean pore size diameter was calculated by BJH method applied to the desorption curve.

Powder X-ray diffraction (XRD) patterns were recorded in Bragg–Brentano parafocusing geometry using a Bruker D5000 diffractometer, equipped with a Cu Kα anode and a graphite monochromator. The XRD data were generally collected in the angular range 10–80° in 2θ using a 0.05° step size and a counting time of 10 s per step. The assignment of the various crystalline phases was based on the JCPDS powder diffraction file cards [38].

The X-ray photoelectron spectroscopy (XPS) analyses of the fresh and spent catalysts were performed with a VG Microtech ESCA 3000 Multilab, equipped with a dual Mg/Al anode. The spectra were excited by the unmonochromatised Al Kα source (1486.6 eV) run at 14 kV and 15 mA. The analyser operated in the constant analyser energy (CAE) mode. Survey spectra were measured at 50 eV pass energy. For the individual peak energy regions, a pass energy of 20 eV set across the hemispheres was used. The sample powders were pelletized and mounted on a double-sided adhesive tape. The pressure in the analysis chamber was in the range of 10^{-8} Torr during data collection. The constant charging of the samples was corrected by referencing all the energies to the C1s peak energy set at 285.1 eV, arising from adventitious carbon. The invariance of the peak shapes and widths at the beginning and at the end of the analyses ensured absence of differential charging. Analyses of the peaks were performed with the software provided by VG, based on non-linear least squares fitting program using a weighted sum of Lorentzian and Gaussian component curves after background subtraction according to Shirley [39] and Sherwood [40]. Atomic concentrations were calculated from peak intensity using the sensitivity factors provided with the software. The binding energy values are quoted with a precision of ±0.15 eV and the atomic percentage with a precision of ±10%. XPS analyses were carried out also on the used catalysts.

Transmission electron microscopy (TEM) was performed on the fresh and spent catalysts by using a JEOL 2010 instrument working at 200 kV equipped with energy-dispersive spectrometer (EDS) for electron probe microanalysis. Suspensions of the samples in ethanol were dropped on carbon-coated grid and after evaporating the solvent electron micrographs of the particles were taken.

2.3. Catalytic tests

Catalytic activity measurements were carried out in a tubular fixed-bed reactor under the reactive gas mixture containing 1000 ppm of C_3H_6 and 9% O_2 in He. The total gas flow rate was 7.2 L h^{-1} and the amount of catalyst was 0.2 g, equivalent to a gas hourly space velocity (GHSV) of 35,000 h^{-1}. In a typical experiment the fresh catalyst (with grain diameters between 50 and 100 μm) was loaded onto a fine-quartz fritted disk and the reaction temperature was continuously monitored by a thermocouple inserted inside the furnace. Each catalytic run was performed as follows: introduction of the reaction mixture at room temperature, heating at a rate of 1 °C/min up to the final temperature of 350 °C (holding 1 h at constant temperature), then cooling down under the reaction mixture. This sequence was repeated for three times. The reactants and products were analysed by gas chromatography, using a dual CTR1 column from Alltech (Porapak and molecular sieve) and a TCD for CO, O_2 and CO_2. A Porapak column and a FID were employed for C_3H_6 detection. In addition, CO_2 was continuously measured on-line by IR analyser (ROSEMOUNT Binos 1004). The only reaction products were CO_2 and H_2O. After three consecutive runs in propene oxidation, the catalysts were recovered for XPS and TEM characterizations (spent catalysts).

3. Results and discussion

Morphological and structural data of gold supported catalysts are listed in Table 1. The X-ray diffraction patterns of fresh gold catalysts are shown in Fig. 1 in the angular range 30–50° 2θ. The specific surface area was ~50 m^2/g for Au/TiO_2 and Au/ZnO, while Au/Al_2O_3 showed much higher surface area (253 m^2/g). All the supports are mesoporous with pore diameters between 10 and 30 nm and pore volume in the range of 0.3–0.7 cm^3/g.

Crystalline features of anatase and rutile phases were observed for Au/TiO_2. For Au/ZnO all diffraction peaks can be indexed to the hexagonal phase ZnO, while in the case of Au/Al_2O_3 features of γ-Al_2O_3 are present. No diffraction lines of metallic Au clusters, at ~38.2° 2θ (1 1 1) and at ~44.4° 2θ (2 0 0) were detected, suggesting the presence of highly dispersed gold crystallites (size < 5 nm) in

Table 1
Morphological and structural data of fresh Au supported catalysts.

Catalyst	BET (m^2/g)	Mean pore diameter (nm) (BJH)	Cumulative pore volume (cm^3/g)	Crystalline phases (XRD)
Au/TiO_2	50	30	0.35	Anatase/rutile
Au/ZnO	48	19	0.30	ZnO
Au/Al_2O_3	253	10	0.70	γ-Al_2O_3

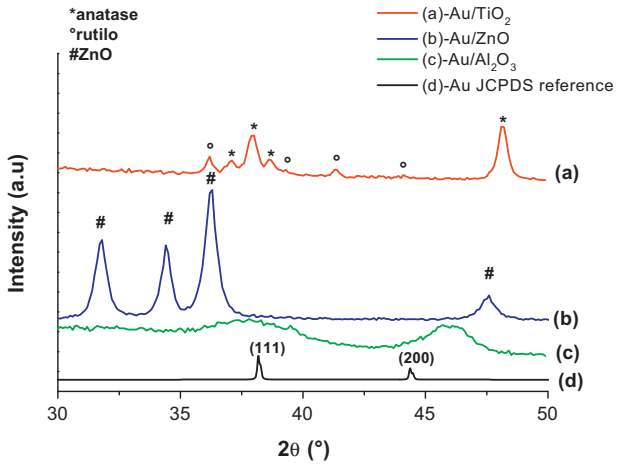

Fig. 1. XRD patterns of fresh Au supported catalysts in the angular range 30–50° 2θ.

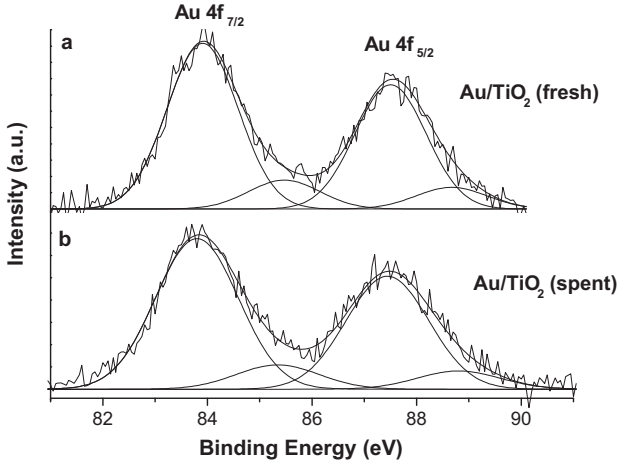

Fig. 2. Au 4f spectra of Au/TiO_2 as (a) fresh and (b) spent catalyst.

the fresh samples. However, for gold over titania and alumina we cannot exclude the presence of broad Au reflections which would be indistinguishable from the large overlapping peaks attributed to anatase and γ-Al_2O_3 phases.

The chemical surface composition of gold supported catalysts was investigated by XPS analyses. In Table 2 the XPS results of fresh catalysts and after propene oxidation runs (spent catalysts) are summarized in terms of the Au $4f_{7/2}$ binding energy (BE) and of the support elements' main peak. The XPS Au 4f spectra of Au/ZnO and Au/Al_2O_3, as fresh and spent catalysts, show a single component at B.E. 84.0 ± 0.3 eV typical of metallic gold [24] The presence of metallic gold is consistent with the reduction treatment, under hydrogen, performed on the prepared catalysts. According to the literature, reduction of gold occurs during propene oxidation [41,42]. Moreover, activation of gold catalysts under hydrogen is beneficial to the propene oxidation indicating that metallic gold is required for the reaction [41,43].

Only in the case of fresh Au/TiO_2, two components at 83.9 eV and 85.5 eV, respectively, typical of Au^0 (85%) and Au^{1+} (15%) were found. According to our previous results [31], 13% of Au^{1+} species, which likely diffuse at the interface with the titania support, remain unreduced in the spent Au/TiO_2 catalyst. In Fig. 2a and b the experimental and fitted Au 4f XPS spectra of Au/TiO_2 (fresh and spent catalysts) are shown.

The surface atomic ratios between gold and the support elements are listed in Table 2 along with the analytical values given in parenthesis. A gold enrichment at the surface was observed for Au/TiO_2, suggesting the presence of highly dispersed gold nanoparticles at the surface of such catalysts. While, smaller gold concentrations were detected on Au/ZnO and Au/Al_2O_3. For all catalysts, the gold signal at the surface decreased noticeably upon three consecutive catalytic runs, with the lowest concentration for Au/Al_2O_3. According to the porous texture of the supports it is likely that such a decrease can be attributed to a temperature-driven inward diffusion of gold nanoparticles, although gold aggregation induced by the reaction temperature cannot be excluded, especially for Au supported over inert alumina.

In order to get more insights into the modification of the chemical surface composition of the catalysts induced by the propene

Table 2
XPS binding energies of gold and main support peaks for fresh and spent (after three catalytic runs) catalysts. For Au/TiO_2 data after a first catalytic run are also enclosed. The atomic percentages of each species are given in parentheses. The surface atomic ratios of gold over support elements (Au/Me) are also reported. For comparison in brackets the analytical ratios Au/Me are given.

Catalyst	Au $4f_{7/2}$ (eV)(at%)	Ti $2p_{3/2}$ (eV)	Zn $2p_{3/2}$ (eV)	Al 2p (eV)	Au/Me[a]
Au/TiO_2 fresh	83.9 (85%) 85.5 (15%)	459.0 (100%)	–	–	0.08 (0.004)
Au/TiO_2 After first run	84.0 (86%) 85.7 (14%)	459.0 (100%)	–	–	0.03
Au/TiO_2 spent	83.9 (87%) 85.7 (13%)	459.0 (100%)	–	–	0.02
Au/ZnO fresh	84.3 (100%)	–	1021.1 (95%) 1022.3 (5%)	–	0.026 (0.004)
Au/ZnO spent	84.0 (100%)	–	1021.1 (96%) 1022.3 (4%)	–	0.009
Au/Al_2O_3 fresh	84.0 (100%)	–	–	75.2 (100%)	0.007 (0.003)
Au/Al_2O_3 spent	84.3 (100%)	–	–	75.1 (100%)	0.002

[a] Me = Ti, Zn, Al.

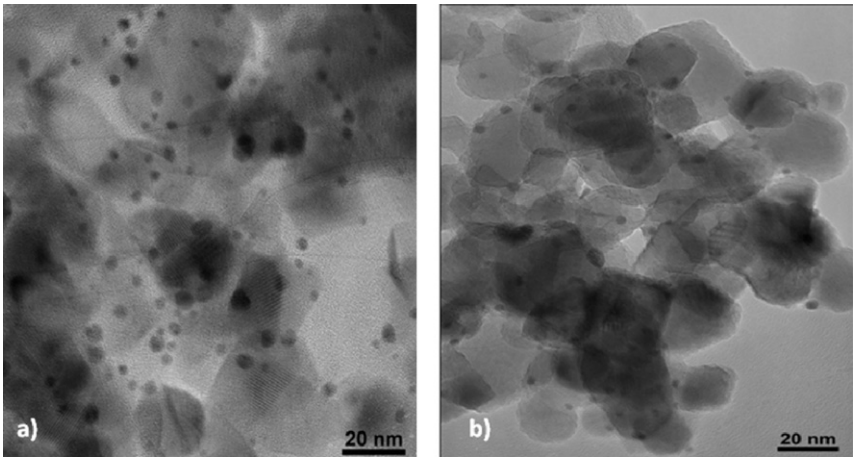

Fig. 3. TEM images of Au/TiO_2 as (a) fresh and (b) spent catalyst.

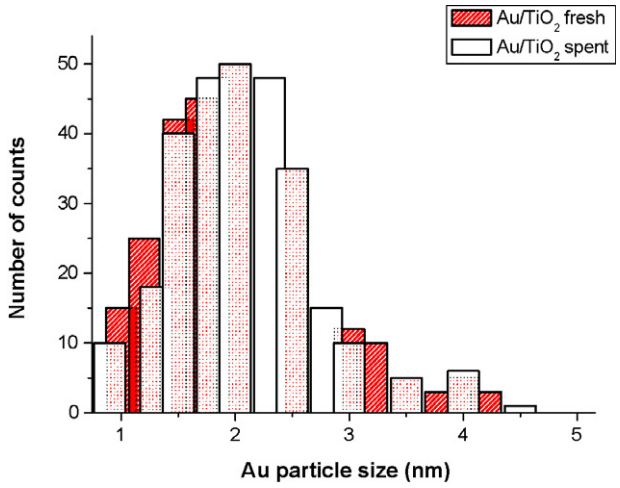

Fig. 4. Statistical analysis of the average particle size of Au/TiO_2 fresh and spent catalyst.

oxidation, XPS analysis was performed on the most active catalyst Au/TiO_2 by recovering it at the end of the first run (see Table 2). No significant differences were observed in terms of B.E. by comparing the catalyst as fresh, after one and after three runs. A decreased gold concentration at the surface was detected also in the sample recovered after one test. By comparing the Au/Ti atomic ratios, it results that surface gold concentration significantly decreased after the first catalytic run then getting stable.

For each catalyst, the support element main peak binding energies, $Ti2p_{3/2}$, Al2p and $Zn2p_{3/2}$ are typical of the corresponding pure oxides, TiO_2, Al_2O_3 and ZnO [44]. The XPS Zn 2p spectra were deconvoluted into two peaks. The dominant component (95%) at 1021.1 eV was associated with the Zn^{2+} in ZnO, while the secondary component (5%) at 1022.3 eV was associated with a zinc hydroxide species [45]. Such species, still detected in the spent sample (4%), are present only on the surface of the catalyst, since no $Zn(OH)_2$ phases were detected by XRD. Presence of a zinc hydroxide species could be related to the specific preparation method of such samples and suggests the presence of defective sites at the surface of the catalyst with a potential positive effect in catalysis [45].

TEM images of fresh and spent catalysts were taken for examining metal nanoparticles and their changes after reaction. In Figs. 3, 5 and 7, representative micrographs of Au/TiO_2, Au/ZnO and Au/Al_2O_3 are displayed, respectively. In Figs. 4, 6, 8 the statistical analyses of the average Au particles size of the above mentioned catalysts are shown. The average particle sizes of fresh and spent Au/TiO_2 samples were 2.0 and 2.3 nm, respectively, according to previous results on AUROlite™ catalysts [35,46]. In the case of Au/ZnO, a slightly larger Au particle diameter, centred at 2.5 nm, was found for the fresh sample, whereas for the spent catalyst the particle size shifted to 3.1 nm. For Au/Al_2O_3 it appears clearly that

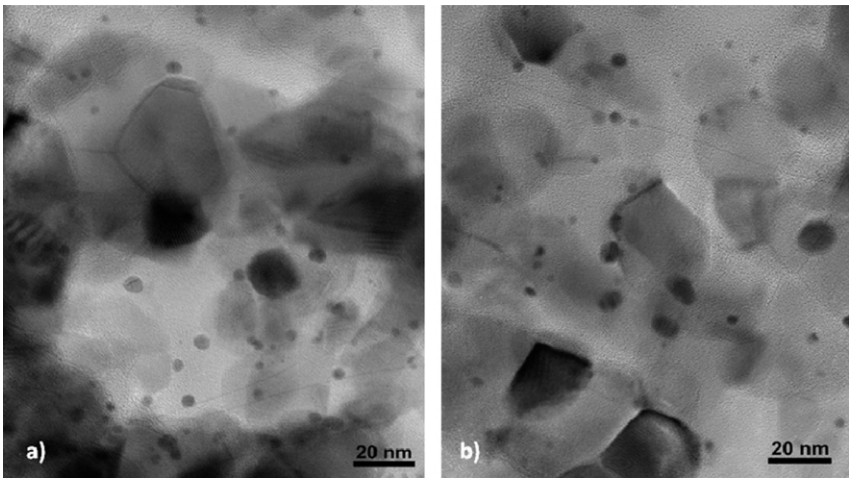

Fig. 5. TEM images of Au/ZnO as (a) fresh and (b) spent catalyst.

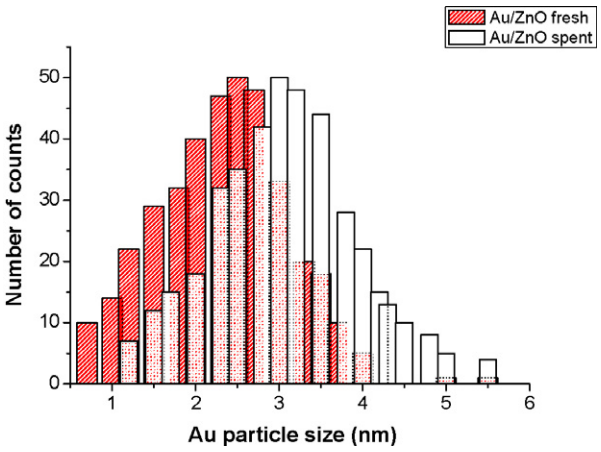

Fig. 6. Statistical analysis of the average particle size of Au on ZnO fresh, and spent catalyst.

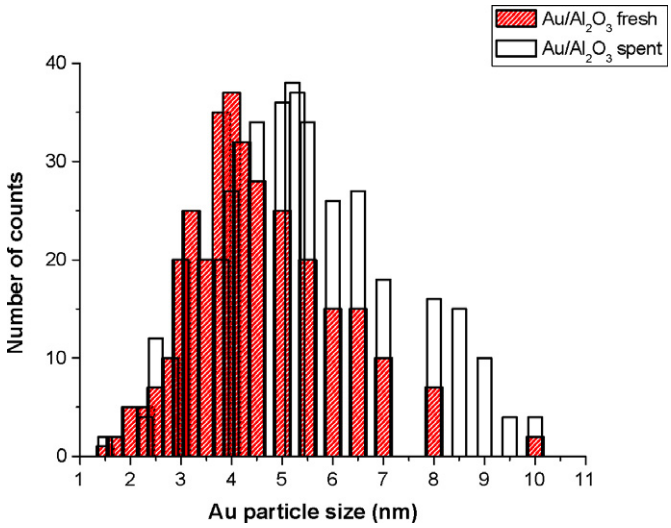

Fig. 8. Statistical analysis of the average particle size of Au on Al_2O_3 fresh and spent catalyst.

Table 3
Temperature (°C) in correspondence to 50% (T_{50}) and 100% (T_{100}) propene conversion during the first and third catalytic runs. The data related to the third run are in brackets. Reaction mixture: 1000 ppm C_3H_6 + 9 vol% O_2 in He, GHSV of 35,000 h^{-1}.

Catalyst	T_{50} (°C)	T_{100} (°C)
Au/TiO_2	242 (263)	290 (320)
Au/ZnO	254 (275)	325 (350)
Au/Al_2O_3	286 (300)	350 (>350)

the distribution of gold particles was heterogeneous and that big crystallites were present. The average Au size was 4.0 nm in the fresh catalyst, whereas the spent sample was found to be larger, 5.3 nm. These findings confirm that gold over a non-reducible oxide, like Al_2O_3 has a tendency to sinter [42].

The catalytic performances of Au/TiO_2, Au/ZnO and Au/Al_2O_3 catalysts were tested in propene oxidation, focusing the attention on the maintenance of the activity by performing three consecutive runs. In Fig. 9a–c the propene conversion curves to CO_2 versus temperature are shown. In Table 3 the temperatures (°C) in correspondence of 50% (T_{50}) and 100% (T_{100}) of propene conversion during the first and third run, respectively, are listed. Looking at the conversion curves, for all catalysts a deactivation occurs after the first run, then no important differences between the second and third run were observed. Au/TiO_2 was the most efficient catalyst followed by Au/ZnO, while Au/Al_2O_3 was the worst performing. The reaction started at around 200 °C and full propene conversion was achieved below 350 °C over both, Au/TiO_2 and Au/ZnO, during all the consecutive runs. The catalytic performances registered for such catalysts compared favourably with literature results [42,43,47].

High dispersion of gold on reducible oxides plays a fundamental role in the activity in VOC oxidation [2,3,41,42]. The presence of nanosized gold metal particles (2 nm), likely interacting with surface titania defects, is consistent with the good activity in propene oxidation and confirms that propene oxidation is a reaction sensitive to the metal structure [41,43]. Moreover, the presence of ionic gold species stabilized at the interface with the titania support, likely enhances the catalytic performances [48,49].

Alumina, a non-reducible and not interacting oxide, yields poor catalytic activity and bigger gold particles (4.0 nm) with limited thermal stability (Au particle size 5.3 nm in the spent catalyst).

Au/ZnO, more active than Au/Al_2O_3, but less performing than Au/TiO_2, contains small Au particles size (2.5 nm) which moderately sintered during reaction (3.1 nm). Moreover, it is likely that the presence of surface defects on the zinc oxide, as deduced by XPS, enhances propene oxidation with respect to Au/Al_2O_3, by promoting oxygen chemisorption or influencing the orientation of gold nanoclusters. The occurrence of a metal–support interaction for

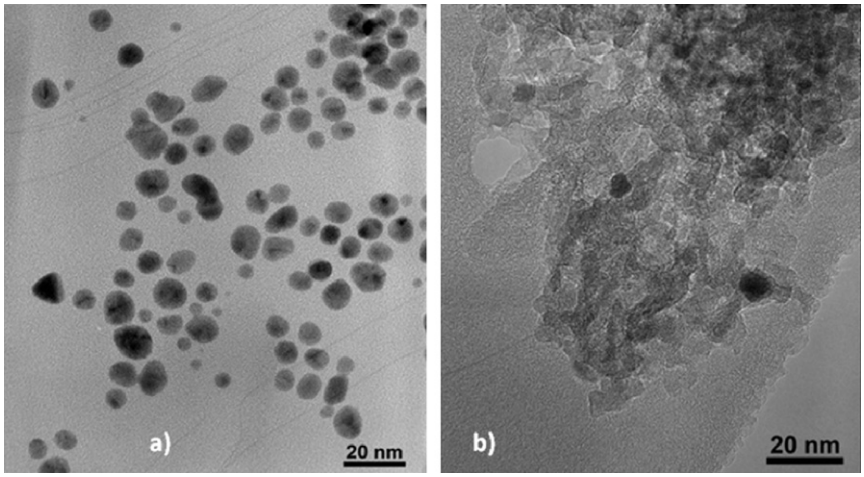

Fig. 7. TEM images of Au/Al_2O_3 as (a) fresh and (b) spent catalyst.

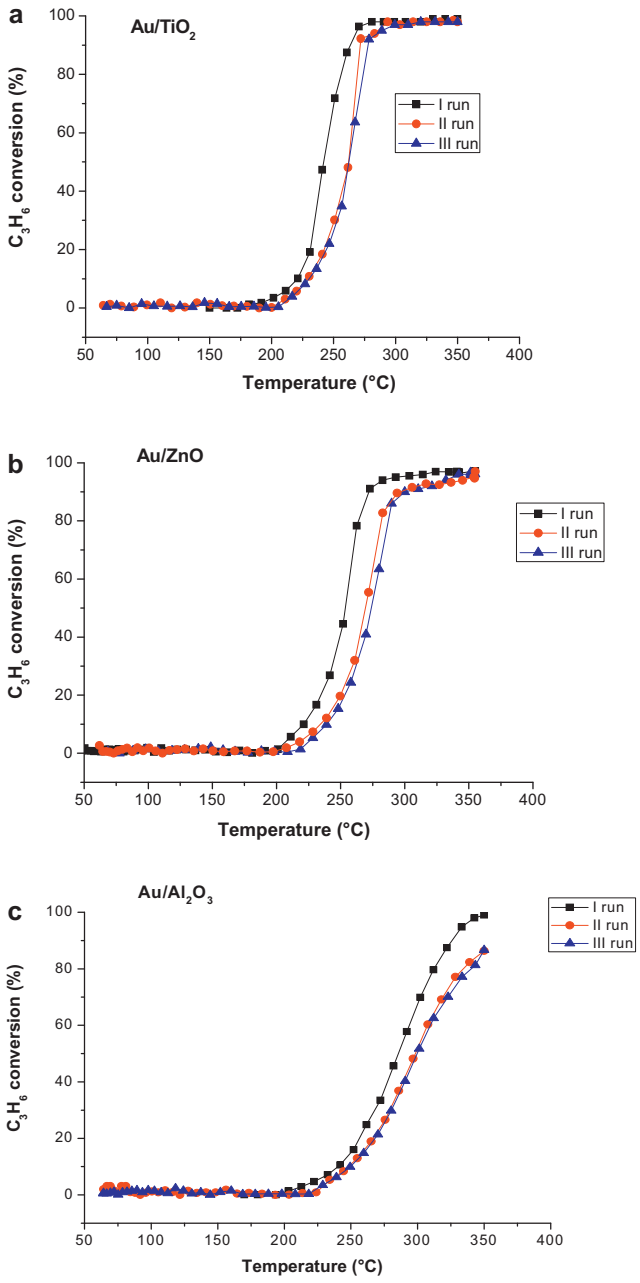

Fig. 9. Conversion (%) of propene versus temperature during three consecutive catalytic runs over (a) Au/TiO_2, (b) Au/ZnO, (c) Au/Al_2O_3 catalysts.

Au/ZnO catalysts has been recently claimed by several authors to explain the high oxidation activity of such systems [15,20,50].

Looking at the maintenance of the activity by carrying out three consecutive runs, all catalysts suffer some deactivation after the first run and then achieved stable conversion in the second and third runs. Au/Al_2O_3 showed the highest deactivation. On the basis of XPS and TEM characterizations of fresh and spent catalysts, we may conclude that the porous morphology of the supports caused inward diffusion of gold nanoparticles within the pores with consequent catalytic deactivation. For Au/Al_2O_3 catalyst gold aggregation also contributed to the decreased catalytic activity. The finding that the XPS gold concentration in Au/TiO_2 decreased after the first run then getting quite stable value is in agreement with the trend of propene conversion. On this basis we can speculate that the main structural modification occurs after the first catalytic run also for Au/ZnO and Au/Al_2O_3 catalysts.

4. Conclusion

In this work we have investigated the propene oxidation performances of Au supported catalysts over three mesoporous oxides characterized by surface area of ~50 m^2/g for titania and zinc oxide, 253 m^2/g for alumina and pore diameter ranging between 10 and 30 nm. The catalysts were characterized by specific surface area measurements (BET method) and pore size distribution, X-ray diffraction (XRD), transmission electron microscopy (TEM) and X-ray photoelectron spectroscopy (XPS) techniques. The evolution of the activity by performing three consecutive runs from room temperature up to 350 °C was correlated to the morphological properties of the supports as well as to the structural and electronic properties of the catalysts as a function of the support. To evaluate the catalysts modification upon reaction, analyses by XPS and TEM techniques were performed on the spent samples.

Au/TiO_2, containing highly dispersed Au^0 nanoparticles (2 nm) strongly interacting with the support was the best performing in the oxidation of propene and maintained stable particle size after reaction. Moreover, the presence of Au^+ species stabilized at the interface with the titania likely enhances the catalytic performances.

Au/ZnO, characterized by metallic gold particles with sizes around 2.5 nm was slightly less performing then Au/TiO_2 in propene oxidation. The presence of surface defects on the zinc oxide may induce a metal–support interaction which stabilizes gold against dramatic sintering.

The presence of bigger Au^0 particles (4 nm) over Al_2O_3 confirms the idea that gold over an inert oxide has poor catalytic activity and tendency to sinter.

In conclusion, this study evidenced that the main requisite to attain high activity in propene oxidation is the occurrence of a metal–support interaction leading to both, nucleation of small gold particles at the surface defects of the support and the stabilization of ionic gold species at the interface with the support.

The achievement of stable catalytic performance is dependent on the nature of the support, interacting or not as well as to the morphology. An inward diffusion of gold nanoparticles within the porous structure of the support was responsible of the observed deactivation during consecutive catalytic runs.

Acknowledgements

The authors gratefully acknowledge Mintek Corporation for supplying gold catalysts and thank F. Giordano (ISMN-CNR, Palermo) for XRD characterization.

References

[1] J.J. Spivey, Ind. Eng. Chem. Res. 26 (1987) 2165.
[2] M.A. Centeno, M. Paulis, M. Montes, J.A. Odriozola, Appl. Catal. A 234 (2002) 65.
[3] D. Andreeva, R. Nedyalkova, M.V. Abrashev, Appl. Catal. A 246 (2003) 29.
[4] A.C. Gluhoi, S.D. Lin, B.E. Nieuwenhuys, Catal. Today 90 (2004) 175.
[5] A.C. Gluhoi, N. Bogdanchikova, B.E. Nieuwenhuys, J. Catal. 229 (2005) 154.
[6] C. Della Pina, N. Dimitratos, E. Falletta, M. Rossi, A. Siani, Gold Bull. 40 (2007) 67.
[7] M.I. Domínguez, M. Sánchez, M.A. Centeno, M. Montes, J.A. Odriozola, J. Mol. Catal. A 277 (2007) 145.
[8] S.Y. Liu, S.M. Yang, Appl. Catal. A 334 (2008) 92.
[9] G.C. Bond, C. Louis, D.T. Thompson, in: G.J. Hutchings (Ed.), Catalysis by Gold, vol. 6, Imperial College Press, London, 2006.
[10] F. Boccuzzi, A. Chiorino, S. Tsubota, M. Haruta, Catal. Lett. 29 (1994) 225.
[11] G.J. Hutchings, M.R.H. Siddiqui, A. Burrows, C.J. Kiely, R. Whyman, J. Chem. Soc., Faraday Trans. 93 (1997) 187.
[12] G.Y. Wang, W.X. Zhang, H.L. Lian, D.Z. Jiang, T.H. Wu, Appl. Catal. A: Gen. 239 (2003) 1.
[13] S. Al-Sayari, A. Carley, S. Taylor, G. Hutchings, Top. Catal. 44 (2007) 123.
[14] M. Comotti, W.-C. Li, B. Spliethoff, F. Schuth, J. Am. Chem. Soc. 128 (2006) 917.
[15] K. Qian, W. Huang, J. Fang, S. Lv, B. He, Z. Jiang, S. Wei, J. Catal. 255 (2008) 269.
[16] F. Boccuzzi, A. Chiorino, S. Tsubota, M. Haruta, Sens. Actuators B: Chem. 25 (1995) 540.

[17] S.-J. Chang, T.-J. Hsueh, I.-C. Chen, B.-R. Huang, Nanotechnology 19 (2008) 175502.
[18] R.K. Joshi, Q. Hu, F. Am, N. Joshi, A. Kumar, J. Phys. Chem. C 113 (2009) 16199.
[19] C. Wongchoosuk, S. Choopun, A. Tuantranont, T. Kerdcharoen, Mater. Res. Innov. 13 (2009) 185.
[20] H. Wu, L. Wang, J. Zhang, Z. Shen, J. Zhao, Catal. Comm. 12 (2011) 859.
[21] M. Comotti, W.C. Li, B. Spliethoff, F. Schüth, J. Am. Chem. Soc. 128 (2006) 917.
[22] M.A. Centeno, C. Portales, I. Carrizosa, J.A. Odriozola, Catal. Lett. 102 (2005) 289.
[23] W.Y. Hernández, F. Romero-Sarria, M.A. Centeno, J.A. Odriozola, J. Phys. Chem. C 114 (2010) 10857.
[24] A.M. Venezia, G. Pantaleo, A. Longo, G. Di Carlo, M.P. Casaletto, L.F. Liotta, G. Deganello, J. Phys. Chem. B 109 (2005) 2821.
[25] L.F. Liotta, G. Di Carlo, G. Pantaleo, A.M. Venezia, Catal. Today 158 (2010) 56.
[26] M.M. Schubert, S. Hackenberg, A.C. van Veen, M. Muhler, V. Plazak, R.J. Behm, J. Catal. 197 (2001) 113.
[27] L. Guczi, G. Peto, A.B.K. Frey, O. Geszti, G. Molnar, C. Daroczi, J. Am. Chem. Soc. 125 (2003) 4332.
[28] Y.-S. Chi, H.-P. Lin, C.-Y. Mou, Appl. Catal. A 284 (2005) 199.
[29] J.A. Hernandez, S. Gómez, B. Pawelec, T.A. Zepeda, Appl. Catal. B 89 (2009) 128.
[30] M.G. Cutrufello, E. Rombi, C. Cannas, M. Casu, A. Virga, S. Fiorilli, B. Onida, I. Ferino, J. Mater. Sci. 44 (2009) 6644.
[31] E. Rombi, M.G. Cutrufello, C. Cannas, M. Casu, D. Gazzoli, M. Occhiuzzi, R. Monaci, I. Ferino, Phys. Chem. Chem. Phys. 11 (2009) 593.
[32] A. Beck, A. Horváth, G. Stefler, R. Katona, O. Geszti, Gy. Tolnai, L.F. Liotta, L. Guczi, Catal. Today 139 (2008) 180.
[33] L. Escamilla-Perea, R. Nava, B. Pawelec, M.G. Rosmaninho, C.L. Peza-Ledesma, J.L.G. Fierro, Appl. Catal. A 381 (2010) 42.
[34] M.P. Casaletto, A. Longo, A.M. Venezia, A. Martorana, A. Prestianni, Appl. Catal. A 302 (2006) 309.
[35] XXX http://www.mintek.co.za.
[36] A. Zwijnenburg, A. Goossens, W.G. Sloof, M.W.J. Crajé, A.M. van der Kraan, L. Jos de Jongh, M. Makkee, J.A. Moulijn, J. Phys. Chem. B 106 (2002) 9853.
[37] R. Zanella, S. Giorgio, C.-H. Shin, C.R. Henry, C. Louis, J. Catal. 222 (2004) 357.
[38] JCPDS Powder Diffraction File, PDF-2 Database, Int. Centre for Diffraction Data, Swarthmore, USA, 2010.
[39] D.A. Shirley, Phys. Rev. B 5 (1972) 4709.
[40] P.M.A. Sherwood, in: D. Briggs, M.P. Seah (Eds.), Practical Surface Analysis, Wiley, New York, 1990, p. 181.
[41] L. Delannoy, K. Fajerwerg, P. Lakshmanan, C. Potvin, C. Méthivier, C. Louis, Appl. Catal. B 94 (2010) 117.
[42] M. Ousmane, L.F. Liotta, G. Di Carlo, G. Pantaleo, A.M. Venezia, G. Deganello, L. Retailleau, A. Boreave, A. Giroir-Fendler, Appl. Catal. B 101 (2011) 629.
[43] A. Baylet, C. Capdeillayre, L. Retailleau, J.L. Valverde, P. Vernoux, A. Giroir-Fendler, Appl. Catal. B: Environ. 102 (2011) 180.
[44] J.F. Moulder, W.F. Stickle, P.E. Sobol, K.D. Bomben, in: J. Chastain, R.C. King Jr. (Eds.), Handbook of X-ray Photoelectron Speectroscopy, Phys. Electronics Inc., Eden Prairie, USA, 1995.
[45] S. Sepulveda-Guzmana, B. Reeja-Jayan, E. de la Rosa, A. Torres-Castro, V. Gonzalez-Gonzalez, M. Jose-Yacaman, Mater. Chem. Phys. 115 (2009) 172.
[46] G. Walther, L. Cervera-Gontard, U.J. Quaade, S. Horch, Gold Bull. 42 (2009) 13.
[47] C. Gennequin, M. Lamallem, R. Cousin, S. Siffert, F. Aïssi, A. Aboukaïs, Catal. Today 122 (2007) 301.
[48] G.C. Bond, D.T. Thompson, Gold Bull. 33 (2000) 41.
[49] L. Delannoy, N. Weiher, N. Tsapatsaris, A.M. Beesley, L. Nchari, L.M. Sven Schroeder, C. Louis, Top. Catal. 44 (2007) 263.
[50] S.A.C. Carabineiro, B.F. Machado, R.R. Bacsa, P. Serp, G. Dražić, J.L. Faria, J.L. Figueiredo, J. Catal. 273 (2010) 191.